Geophysical Journal International

Geophys. J. Int. (2023) **233,** 2039–2052
Advance Access publication 2023 January 23
GJI Gravity, Geodesy and Tides

https://doi.org/10.1093/gji/ggad026

Glacial isostatic adjustment in the northern adriatic region: estimates of the contribution from the Alpine ice sheet

Fernando Linsalata [1], Daniele Melini [2] and Giorgio Spada [1]

[1] *Dipartimento di Fisica e Astronomia (DIFA), Alma Mater Studiorum Università di Bologna, Viale Carlo Berti Pichat* 8, 40127, *Bologna, Italy.*
*E-mail: f.linsalata*91*@gmail.com*
[2] *Istituto Nazionale di Geofisica e Vulcanologia, Sezione di Sismologia e Tettonofisica,Via di Vigna Murata* 605, *I*-00143 *Roma, Italy*

Accepted 2023 January 17. Received 2023 January 17; in original form 2022 September 6

SUMMARY

The present-day sea-level variations and vertical movements in the northern Adriatic Sea and in the highly vulnerable Venetian Lagoon result from a number of simultaneously operating contributions. These include Glacial Isostatic Adjustment (GIA), the global, long-term process arising from interactions between the cryosphere, the solid Earth and the oceans in response to the melting of continental ice sheets. Although the GIA contribution in northern Adriatic Sea has been the subject of various investigations so far, significant uncertainties still exist, especially related to the extent and chronology of the Würm Alpine ice sheet and to the rheological profile of the mantle. Here, taking advantage of the recent publication of updated deglaciation chronologies for the far field late-Pleistocene ice sheets and for the near-field alpine ice complex, we produce up-to-date estimates of the present-day rates of GIA-induced relative sea-level variations and vertical displacements in the Venetian Lagoon and in the northern Adriatic Sea, which are compared with GNSS and tide-gauge observations. From high-resolution numerical simulations, we find that GIA is responsible for a complex pattern of geodetic signals across the Po plain and the northern Adriatic Sea. The modeled GIA rates are of the order of fractions of mm yr^{-1}, generally small – but not negligible – compared to the signals observed at local tide gauges and at GNSS sites in the Po plain and facing the Venetian Lagoon. Our results indicate that, while GIA represents a relatively small component among those responsible for present-day land movements and relative sea-level variations in the northern Adriatic Sea, its contribution needs to be taken into account for a correct interpretation of the observed geodetic variations.

Key words: Loading of the Earth; Sea level change; Europe; Numerical modelling.

1 INTRODUCTION

The Venetian Lagoon is a shallow coastal inlet located along the Adriatic Sea in northeastern Italy (see Fig. 1), which originated nearly 6000 yr BP at the apex of the Flandrian Transgression (Gatto & Carbognin 1981; Brambati *et al.* 2003). Since then, sea levels have undergone minor oscillations. In this area, the sea-level variations result from a range of simultaneuos, interrelated processes of geodynamical, geological and metereological nature, as recently discussed by Zanchettin *et al.* (2021). Among these, a potentially important contribution is given by Glacial Isostatic Adjustment (GIA), the process arising from the interactions between the cryosphere, the solid Earth and the oceans in response to the melting of ice loads. While sea-level signals caused by tectonic forces may exhibit a complex spatial and temporal variability (see e.g. Carminati & Di Donato 1999; Stocchi & Spada 2007), those associated with GIA are characterized by smooth, long-wavelength patterns (Clark *et al.* 1978; Clark & Lingle 1979). However, Spada & Melini (2022) have shown that the regional variability of GIA in the Mediterranean is significant in spite of the relatively small extent of the basin, demanding the adoption of high resolution models.

Although the GIA contribution in northern Adriatic Sea has been discussed several times, significant uncertainties still exist, especially related with the extent and chronology of the Würm Alpine ice-sheet (from 26 to 9 kyr BP) that, due to its proximity to the Venetian Lagoon and to the coasts of the northern Adriatic, is still affecting the isostatic equilibrium in these particular areas. This was first pointed out by Gudmundsson (1994), who studied the post-glacial rebound process occurring in the Swiss Alps and the surrounding regions using a simplified disc model (see discussion in Spada *et al.* 2009). Following the work of Gudmundsson (1994), Stocchi *et al.* (2005) estimated the effects of melting of the Alpine ice sheet, including relative sea-level and geodetic signals. They focused on the GIA effects in the Po plain and along the coasts of the

Figure 1. Overview of the study area. The dashed box corresponds to the region shown in Fig. 2(a).

Adriatic Sea, extending results by Carminati & Di Donato (1999) who only considered isostatic effects associated with the remote ice sheets, thus neglecting the possible role of the Würm Alpine glacier.

GIA in the northern Adriatic Sea has been the subject of various investigations, sometimes leading to contrasting results. For example, according to the GIA model based upon the K33_j1b_WS9_6 ice sheet history of Lambeck *et al.* (2011), sea-level in Venice raised by about ∼2.2 m over the past 5000 yr, with present-day rates of relative sea-level change of ∼0.4 mm yr^{-1}. Conversely, the ICE-7G_NA (VM7) GIA model by Roy & Peltier (2018) predicts a substantially stable sea-level over the same period, pointing to a negative contribution of GIA to present-day sea-level change. In addition to the different rheological layering assumed in the two GIA models, these discrepancies are to be attributed to differences in the ice sheet chronologies, reflecting our still incomplete understanding of the spatial and temporal evolution of continental ice sheets during last millennia. Besides those global aspects, on the Northern Adriatic scale a major difference exists between those two GIA models. Indeed, ICE-7G_NA does not include glacial loads over the Alps, while models from the Lambeck group contain an Alpine component, albeit it does not provide a detailed and up-to-date description of the evolution of regional ice loads; these differences are the most likely cause of inconsistent estimates of GIA in the Northern Adriatic between the two models.

The availability of updated global GIA models like ICE-7G_NA (VM7) by Roy & Peltier (2015, 2017), which is expected to provide more precise assessments of the ongoing effects of GIA across the Mediterranean Sea (Roy & Peltier 2018) and the recent reconstructions of the Würm ice sheet over the whole last glacial cycle (Seguinot *et al.* 2018), whose implications upon vertical land movements across the Po plain and the surrounding regions have not yet been investigated, motivates a re-evaluation of GIA in the Venetian Lagoon using state-of-the-art numerical models recently developed (Spada & Melini 2019b), which allow a more comprehensive simulation of GIA processes and are able to attain high spatial resolutions. The latter aspect is of particular importance, in view of the narrow geographical extent of the northern Adriatic sea.

This paper is organized as follows. In Section 2 we review previously published results on sea-level change and vertical land motion in the Northern Adriatic and we present our estimates of vertical velocities based on publicly available geodetic time series. In Section 3 we describe our approach to GIA modeling, including the effects of both remote and near-field ice sheets. Our numerical results are presented in Section 4, before discussing their geophysical interpretation in Section 5. Finally, our concluding remarks are outlined in Section 6.

2 SEA-LEVEL CHANGE AND VERTICAL LAND MOTION IN THE NORTHERN ADRIATIC

2.1 Tide gauge and altimetry observations

The Venetian Lagoon covers about 550 km^2 along ∼50 km of low-lying coast within the easternmost boundary of the Po Plain. It is

connected to the northern Adriatic Sea through three tidal inlets, namely Lido, Malamocco and Chioggia (Fig. 1) and is characterized by a marked vulnerability to coastal flooding due to extreme water heights (Lionello *et al.* 2021). The monitoring of sea-level changes in Venice relies on both *in situ* observations recorded by tide gauges and remote sensing data provided by satellite altimetry. Since tide gauges record sea-level relative to the solid Earth, they are expected to be affected significantly by vertical land movements and in particular by GIA (see e.g. Zanchettin *et al.* 2021).

Various estimates for the trend of secular sea-level rise in the Venetian Lagoon have been proposed in the literature. For an in-depth review, the reader is referred to Zanchettin *et al.* (2021). Studies based on instrumental records have generally provided rates between 0.4 and 1.4 mm yr^{-1} (Emery *et al.* 1988; Douglas 1991, 1997; Tsimplis & Spencer 1997; Marcos & Tsimplis 2008). The wide range of estimated rates depends, in part, on the relative duration of the tide gauge records used in these studies but it is also a consequence of anthropogenic factors, mainly the withdrawal of groundwater, which has varied in intensity through time (Buble *et al.* 2010; Zanchettin *et al.* 2021).

In this work, we rely upon the tide gauge data made publicly available by the Permanent Service for Mean Sea Level (PSMSL; http://www.pol.ac.uk/psmsl). Those of Trieste and Venice (Venezia Punta Della Salute) are by far the longest spanning records (Tsimplis *et al.* 2012) in the northern Adriatic Sea (see Fig. 2). For a summary of the record lengths and data availability from other sites, the reader is referred to Galassi & Spada (2014). The Revised Local Reference (RLR) records across the Adriatic Sea share similar temporal patterns, with inter-annual and inter-decadal components showing the same general trends and amplitudes (Galassi & Spada 2014). The overall picture shows that the sea-level behaviour in the Adriatic Sea on these time scales is, to a large extent, uniform (Marcos & Tsimplis 2007). The longest-spanning station of Venice (Venezia Punta Della Salute) shows a trend of (2.4 $\pm$ 0.2) mm yr^{-1}, twice the trend of Trieste of (1.2 $\pm$ 0.1) mm yr^{-1}. Two other tide gauge stations are available in Venice, both operating since early 20th century: Venezia Santo Stefano, with a trend of (2.5 $\pm$ 0.4) mm yr^{-1} (Carbognin *et al.* 2010) and Venezia Arsenale, with a trend of (1.8 $\pm$ 1.0) mm yr^{-1} (Tsimplis *et al.* 2012). Data from these stations are shown in Fig. 2, while rates obtained for each station are compared in Fig. 3. Venezia Santo Stefano is characterized by a rate consistent with the value at Venezia Punta Della Salute, but note that the two records cover time windows that do not overlap. Although the rate of sea-level change at Venezia Arsenale is affected by a very large uncertainty, it is found to be in general agreement with rates from other tide gauges in the Venetian Lagoon. Conversely, the sea-level trend at Trieste is considerably smaller than rates in the Venetian Lagoon; this difference is likely to be the result of high rates of subsidence in the Venice area due to groundwater extraction activities. It is worth noting that the standard error for records longer than 50 yr is less than 0.3 mm yr^{-1} while the two records exceeding 80 yr (namely, Venezia Punta Della Salute and Trieste), have errors $<$0.2 mm yr^{-1} and for shorter records spanning about 25 yr the error is $>$0.6 mm yr^{-1} (Tsimplis *et al.* 2012).

Furthermore, in Venice we have the chance of comparing the rates from tide gauge records with independent sea-level observations. For instance, on the basis of 'photographic' evidence from the Venetian painters, Camuffo & Sturaro (2003) estimated that in the period 1727–2000 the average rate of sea-level rise in the lagoon has been (2.3 $\pm$ 0.4) mm yr^{-1}, consistent with the trends obtained with the longest tide gauge records available. We remark also that a long-term record of relative sea-level change is provided by tidal notches found in the northern Adriatic. The notches, whose age is only poorly determined, are currently located at depths ranging between 0.5 and 0.6 m below current sea-level. If they can be considered as relatively recent, as suggested by similar structures found in Roman jetties (Fouache *et al.* 2000), then they may be consistent with a long term sea-level rise of $\geq$0.3 mm yr^{-1}.

In contrast with the *in situ* observations from tide gauges, satellite altimetry observations are only available since the mid-70s. Their accuracy in estimating sea-surface height has increased considerably in the early 90s with the launch of the TOPEX/Poseidon satellite mission and later with the Jason missions. An overall global-mean rate of absolute sea-level rise of $\approx$3 mm yr^{-1} during the 'altimetry era' (i.e. since year 1992) is reported by several studies (see e.g. Cazenave & Llovel 2010; Cazenave *et al.* 2018). The quantity and quality of altimetry data for the northern Adriatic Sea and in the Venetian Lagoon has been recently thoroughly reviewed by Zanchettin *et al.* (2021), who estimated a trend of absolute sea-level rise of (5.9 $\pm$ 1.4) mm yr^{-1} over the period 1993–2008, at a point in the Adriatic Sea that lies $\sim$80 km away from Venice. In contrast, Rocco (2015) obtained trends of (4.18 $\pm$ 0.92) mm yr^{-1} and of (3.40 $\pm$ 0.99) mm yr^{-1} during time periods 1993–2014 and 1993–2013, respectively, at a point that lies close to the Venetian tide gauges. In their reanalysis over the time period 1993–2015, Vignudelli *et al.* (2019) obtained a trend of (4.03 $\pm$ 1.27) mm yr^{-1} after the removal of the seasonal component (see e.g. Legeais *et al.* 2018). The above rates of absolute sea-level rise obtained for Venice and for the northern Adriatic clearly exceed the global average of $\approx$3 mm yr^{-1} observed by altimetry (Cazenave & Llovel 2010). However, according to global studies, they also exceed (by one order of magnitude) the contribution that we expect from GIA, which according to state-of-the-art models is close to 0.3 mm yr^{-1} when averaged over the oceans (see e.g. Spada 2017; Spada & Melini 2019a). Local predictions, specific for this study, shall be provided in the following using updated GIA models.

2.2 GNSS observations

Vertical land movement (VLM) constitutes a very important contribution to the variability of sea-level in the Venetian Lagoon (Carbognin *et al.* 2009; Zanchettin *et al.* 2021). VLM results from the combination of different components due to tectonics, sediment loading and compaction, GIA and anthropogenic activities (Davis *et al.* 2003; Buble *et al.* 2010). In the Venice area, all these components induce non-negligible displacements although their magnitude and relative importance have changed over time. The net result is a coastal subsidence that exacerbates the effects of climate-driven sea-level rise (Zanchettin *et al.* 2021).

In this study, we have analyzed 45 GNSS time series for the Venetian Lagoon and the surrounding areas, distributed from the Nevada Geodetic Laboratory (NGL) at the University of Nevada, Reno. Details on the data set are available on the NGL webpage (http://geodesy.unr.edu/index.php). Following Kreemer *et al.* (2018), Kreemer & Blewitt (2021) and Michel *et al.* (2021), we considered only time series whose length is at least 2.5 yr. Indeed, according to Blewitt & Lavallée (2002), this is the minimum acceptable length to ensure that estimated trends are not significantly affected by biases due to seasonal components. To estimate vertical velocities from the GNSS time series we use the MIDAS (Median Interannual Difference Adjusted for Skewness) median-trend algorithm introduced by Blewitt *et al.* (2016). We also use the

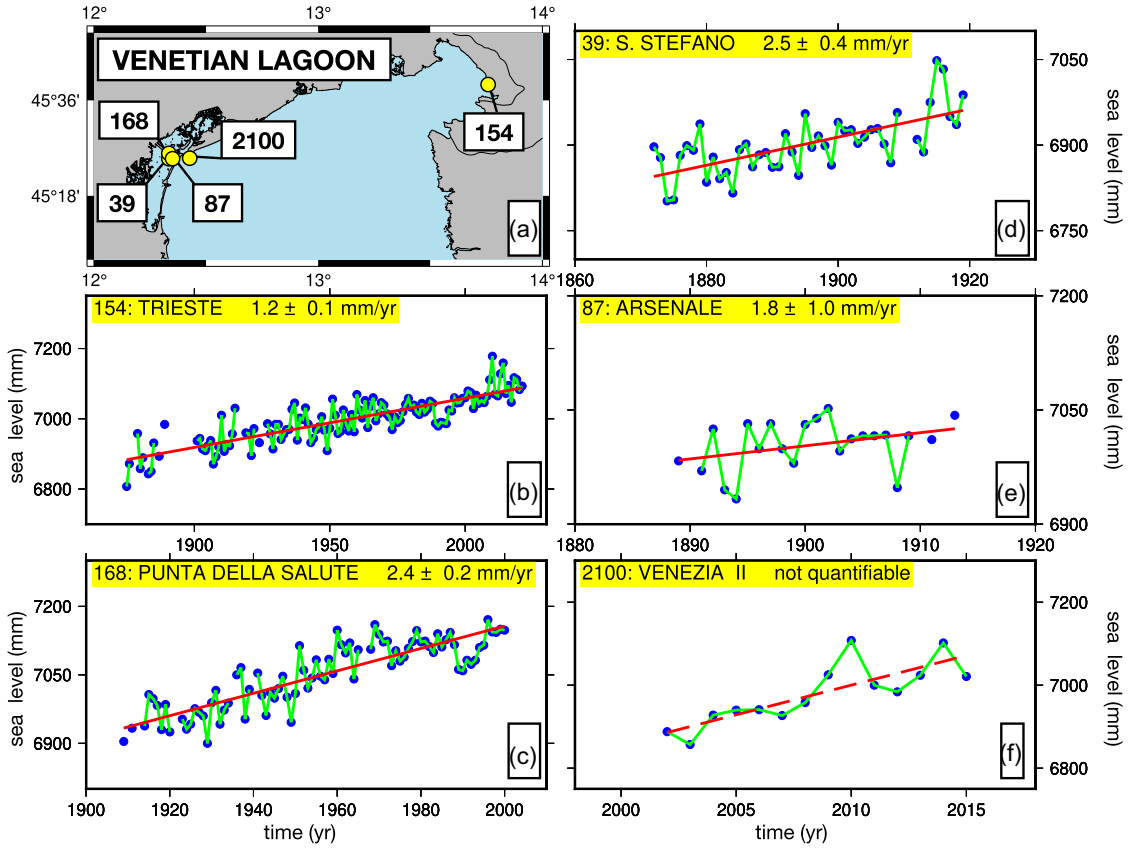

Figure 2. Location of PSMSL tide gauges in the Venetian Lagoon (a) and annual RLR time series for Trieste (c, ID: 154), Venezia Punta Della Salute (d, ID: 168), Venezia Santo Stefano (e, ID: 39), Venezia II (f, ID: 2100) and Venezia Arsenale (g, ID: 87). The red line in panels (b)–(e) is obtained with a linear regression of the tide gauge time series; the corresponding rate of sea-level change is reported in the panel headers. Note that the time ranges are different for frames (c)–(g). Data have been obtained from the PSMSL web page (https://www.psmsl.org).

equipment changes tabulated by NGL from station 'site logs' (i.e. antenna/radome changes and receiver make changes). The MIDAS trend estimator can handle common problems such as step discontinuities, outliers, seasonality, skewness and heteroscedasticity and it represents a variant of the Theil-Sen non-parametric median trend estimator (Theil 1950; Sen 1968). The MIDAS-estimated velocity is essentially the median of the distribution of 1 yr slopes, making it insensitive to the effects of steps in the time series if they are sufficiently infrequent. The uncertainties obtained through the MIDAS algorithm have a realistic meaning and usually do not require further scaling (e.g. Hammond *et al.* 2016; Caron *et al.* 2018; Kreemer & Zaliapin 2018; Yu *et al.* 2018; Ojo *et al.* 2021). Thus, time series length must be greater than 1 yr such that at least one full cycle of periodic seasonal behavior, if it exists, is captured and any transient signals can be distinguished from secular behavior. The differencing of pairs separated by 1 yr minimizes effects with annual periodicity, but not other transient signals with different periodicity as suggested by Murray *et al.* (2019).

Fig. 4 shows the location of the 45 GNSS sites considered in this work, the vertical velocity v we obtained at each site and the associated uncertainty σ_v. Numerical values of $(v \pm \sigma_v)$ for each GNSS site are listed in Table 1. The length of the individual time-series and three MIDAS processing examples are shown in Fig. 5. We note that among those considered in Fig. 4(a), we obtain a positive vertical velocity (i.e. an uplift) at only seven stations out of 45: TREV (0.71 ± 0.87 mm yr^{-1}), VOLT (0.97 ± 0.76 mm yr^{-1}), BASS (0.15 ± 1.36 mm yr^{-1}), MT06 (0.29 ± 1.04 mm yr^{-1}), MT10 (0.68 ± 0.87 mm yr^{-1}), MGRD (0.53 ± 0.57 mm yr^{-1}) and VITT (0.23 ± 0.77 mm yr^{-1}). The map in Fig. 4(a) clearly highlights the diffuse state of subsidence in the Venice region and in the surroundings. Subsidence rates reach the maximum value of (-5.75 ± 2.54) mm yr^{-1} at MST1, in the Mestre Metropolitan City of Venice. Large subsidence rates are also found at TGPO (-5.26 ± 0.65 mm yr^{-1}) and at PTO1 (-5.15 ± 0.76 mm yr^{-1}), in the Po Delta. The weighted average of vertical velocities over all the considered stations is (-1.35 ± 0.10) mm yr^{-1}.

3 GLACIAL ISOSTATIC ADJUSTMENT

In what follows, we discuss our model estimates of GIA in the Northern Adriatic. We considered separately two contributions: *(i)* the effect of global-scale GIA in response to the melting of late-Pleistocene ice sheets, which are located in the far field of the study region and *(ii)* the contribution stemming from the melting of the Alpine ice sheets during the last glacial cycle.

3.1 GIA in response to the melting of far field ice sheets

To model the effects of GIA in the NE Adriatic sea following the melting of far-field ice sheets, we obtained a numerical solution of the Sea Level Equation (SLE), the integral equation describing the interactions between the solid Earth, the oceans and the cryosphere in response to the evolution of surface ice loads. Originally formulated by Farrell & Clark (1976), the SLE accounts for deformational,

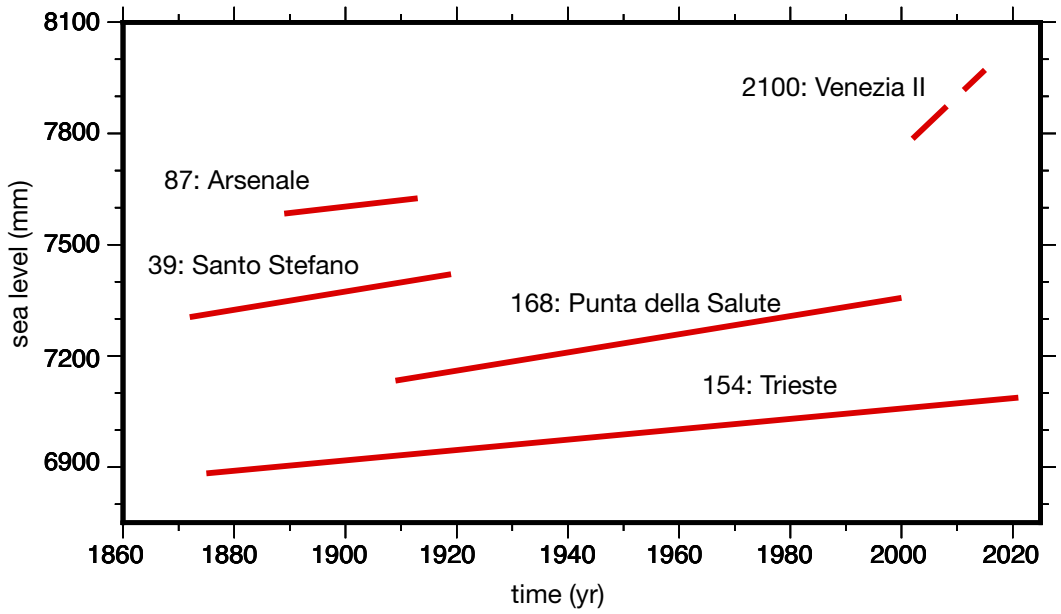

Figure 3. Comparison between sea-level change trends obtained from tide gauge records shown in Fig. 2.

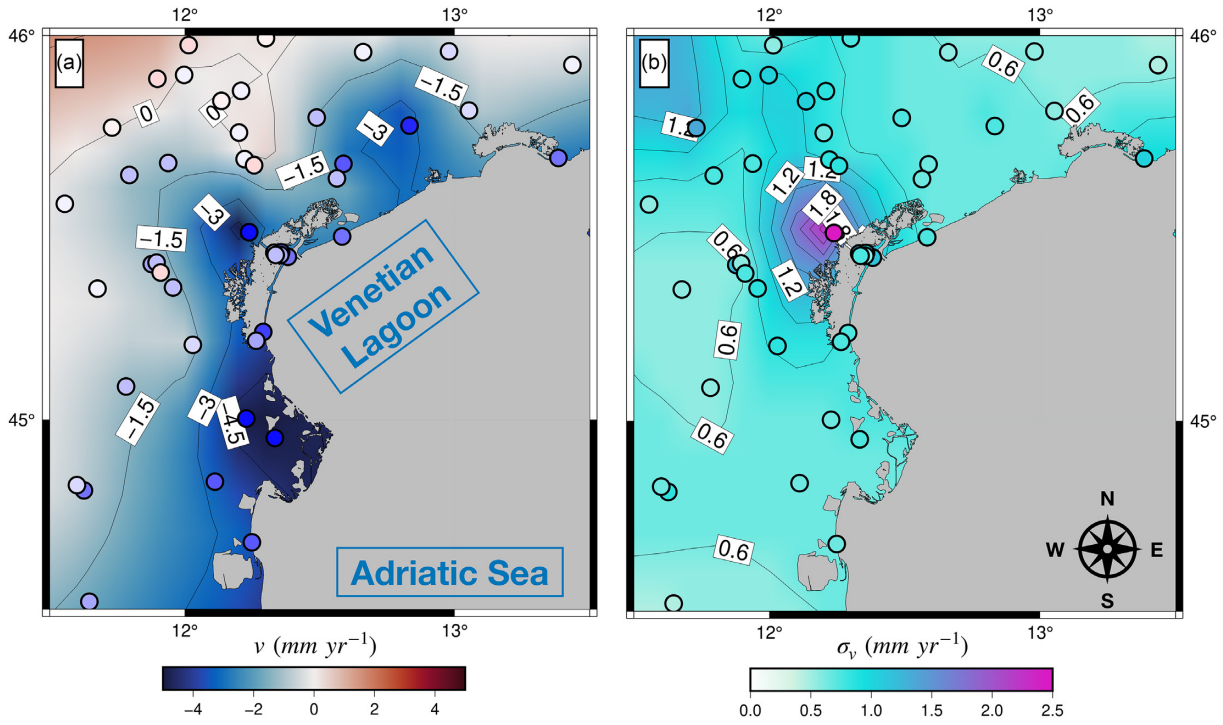

Figure 4. Estimated vertical velocities (v, frame a) and associated uncertainties (σ_v, frame b) at the 45 GNSS sites considered in this work. An interpolated field for v and σ_v is also shown. Please note that the color scale in frame (a) is saturated at ± 5 mm yr^{-1}. The interpolation has been obtained with program `surface`, which is part of the GMT (Generic Mapping Tools) package by Wessel & Smith (1998), employing a tension factor of 0.5.

gravitational and rotational effects induced by spatio-temporal variations of the ice and the meltwater loads (Spada 2017; Whitehouse 2018). In its simplest form, the SLE reads $S(\theta, \lambda, t) = N - U$, where S is the sea-level variation relative to the solid Earth, N is the sea-surface variation (absolute sea-level change) and U is the vertical displacement of the bedrock. These three fields depend upon the location on the Earth surface (colatitude θ and longitude λ) and on time t. As discussed by *e.g.* Spada & Melini (2019b), N and U also implicitly depend upon S, making the SLE an integral equation that can be only solved through numerical iterative methods. Non-linear effects in the SLE arise because of the migration of the shorelines in response to GIA and because of the transition between grounded and marine-based ice that occurred during deglaciation. As a consequence of the SLE, the rate of sea-level change $\dot{S}$, the vertical velocity $\dot{U}$ and the rate of change of absolute sea-level $\dot{N}$ are related by $\dot{S} = \dot{N} - \dot{U}$, regardless the particular combination

Table 1. Vertical velocities estimated with the MIDAS algorithm at the 45 GNSS sites considered in this study and corresponding modeled vertical velocities according to the combined effect of the ICE-7G_NA (VM7) and iALP models.

ID	lon (deg)	lat (deg)	GIA (mm yr^{-1})	MIDAS (mm yr^{-1})	ID	lon (deg)	lat (deg)	GIA (mm yr^{-1})	MIDAS (mm yr^{-1})
BASS	11.73	45.76	+0.44	+0.15 ± 1.36	PORD	12.66	45.95	+0.42	−0.02 ± 0.53
CAFV	11.93	45.67	+0.43	−1.28 ± 0.73	PORT	12.83	45.76	+0.40	−4.12 ± 0.75
CAVA	12.58	45.47	+0.37	−2.54 ± 0.71	PSAL	12.33	45.43	+0.37	−1.11 ± 0.78
CGIA	12.26	45.20	+0.33	−1.84 ± 0.77	PTO1	12.33	44.95	+0.28	−5.15 ± 0.76
CITT	11.79	45.63	+0.43	−1.19 ± 0.72	REBO	12.03	45.19	+0.34	−0.66 ± 0.85
CODI	12.11	44.83	+0.26	−3.23 ± 0.65	ROVI	11.78	45.08	+0.32	−1.28 ± 0.53
CODR	12.97	45.95	+0.41	−0.52 ± 0.53	SDNA	12.56	45.63	+0.38	−1.07 ± 0.65
FER1	11.60	44.82	+0.26	−0.60 ± 0.69	SFEL	12.29	45.23	+0.34	−3.88 ± 0.75
FERA	11.62	44.81	+0.26	−2.99 ± 0.83	SUSE	12.20	45.85	+0.44	−0.26 ± 0.88
GARI	12.24	44.67	+0.22	−3.27 ± 0.63	TEOL	11.67	45.34	+0.37	−0.13 ± 0.54
GRDO	13.38	45.68	+0.35	−2.76 ± 1.00	TGPO	12.22	45.00	+0.29	−5.26 ± 0.65
LERO	11.95	45.34	+0.37	−1.38 ± 0.84	TREV	12.25	45.66	+0.41	+0.71 ± 0.87
MDEA	13.43	45.92	+0.38	−0.43 ± 0.49	TRVS	12.22	45.68	+0.42	−0.02 ± 0.85
MEDI	11.64	44.52	+0.19	−1.79 ± 0.49	UPAD	11.87	45.40	+0.38	−1.55 ± 1.10
MGRD	12.01	45.97	+0.46	+0.53 ± 0.57	VAL7	11.99	45.89	+0.45	−0.12 ± 1.02
MST1	12.23	45.49	+0.38	−5.75 ± 2.54	VEN1	12.35	45.43	+0.37	−1.62 ± 0.56
MT01	12.20	45.74	+0.42	−0.19 ± 0.61	VEN2	12.35	45.43	+0.37	−3.02 ± 0.94
MT06	12.13	45.83	+0.44	+0.29 ± 1.04	VENE	12.33	45.43	+0.37	−1.00 ± 1.23
MT10	11.89	45.88	+0.45	+0.68 ± 0.87	VENI	12.38	45.42	+0.36	−2.73 ± 1.13
NOVE	12.58	45.66	+0.39	−3.02 ± 0.60	VICE	11.55	45.56	+0.42	−0.47 ± 0.59
ODEZ	12.48	45.78	+0.41	−1.49 ± 0.70	VITT	12.30	45.99	+0.45	+0.23 ± 0.77
PADO	11.89	45.41	+0.38	−1.06 ± 0.53	VOLT	11.91	45.38	+0.38	+0.97 ± 0.76
PAZO	13.05	45.80	+0.38	−0.87 ± 0.56					

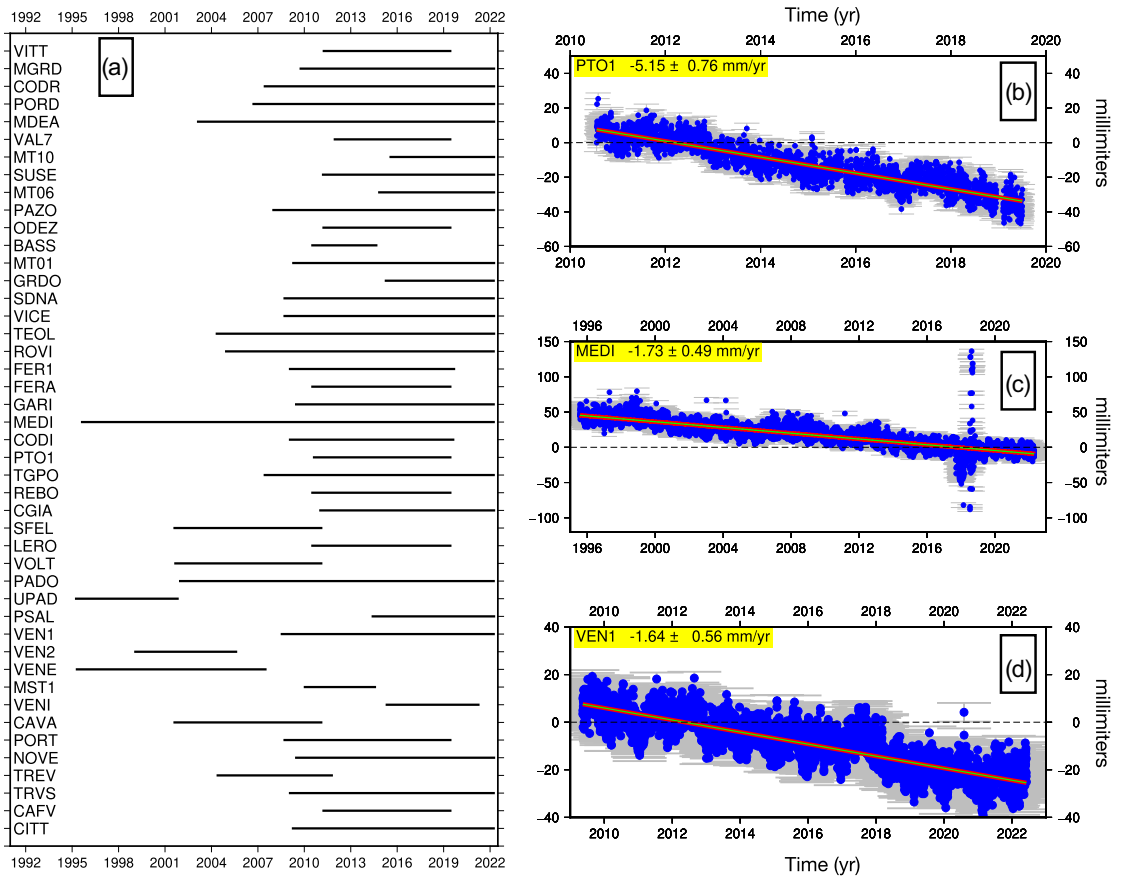

Figure 5. (a) Time windows covered by the 45 GPS time series of vertical displacement considered in this work. Frames (b), (c) and (d) show examples of GPS daily time series, namely the up-component at the PTO1, MEDI and VEN1 sites, respectively. The red line represents the GPS velocity computed by MIDAS (Blewitt *et al.* 2016) and the blue solid circles represent the offset daily coordinate time series. Please note that both horizontal and vertical axes are different in frames (b)-(d).

of rheology and ice model employed and of the rotation theory adopted (Stocchi & Spada 2009).

In this work, we employ the ICE-7G_NA (VM7) GIA model, the latest iteration of the ICE-X suite of global models developed by WR Peltier and collaborators (Roy & Peltier 2015, 2017). The model decribes the spatio-temporal evolution of ice sheets starting from 26 kyrs BP, a spherically symmetric Earth with Maxwell viscoelastic rheology. We implemented the ICE-7G_NA model into the SELEN^4 open-source SLE solver (Spada & Stocchi 2007; Spada & Melini 2019b) by converting the geographical grids available on the home page of WR Peltier into a set of disc-shaped, axisymmetric elements, arranged according to the equal-area icosahedron grid by Tegmark (1996) and assigning a piece-wise constant time history to each element. The SELEN^4 solver has been configured to perform three external iterations in which the evolution of paleo-topography is progressively refined and three internal iterations in which the SLE is numerically solved for a given paleo-topography configuration; for further details about the SLE solution scheme, the reader is referred to Spada & Melini (2019b) and its supplementary material. All the computations are carried out up to harmonic degree $l_{\max} = 128$, which by the Jeans' rule corresponds to a minimum wavelength of about 312 km on the surface of the Earth and employing a resolution parameter R = 100 that corresponds to a global icosahedral grid with a pixel size of about 40 km (for details, see the supplement to Spada & Melini 2019b). This choice of resolution parameters provides an adequate representation of the spatial variability in the far field of late Pleistocene ice sheets, while ensuring a reasonable trade-off between model resolution and computational costs. Present-day topography has been assigned to the icosahederal grid by averaging the bedrock version of the one arc-minute resolution ETOPO1 global relief (Amante & Eakins 2009) over the cell area associated to each pixel. We assume the VM7 rheological profile by Roy & Peltier (2017), which includes a 75 km thick elastic lithosphere, a three-layer upper mantle, a transition zone, a three-layer lower mantle and an inviscid fluid core; the structure of layers and their viscosity values are those listed in table 2 of Roy & Peltier (2017). The rotational feedback on sea-level is taken into account following the revised theory of Mitrovica *et al.* (2005) and Mitrovica & Wahr (2011).

3.2 Regional viscoelastic rebound modeling in the Alps

In previous studies about the role of GIA in the Mediterranean region (see e.g. Stocchi *et al.* 2005), the time evolution of the Alpine ice sheet has been modeled coarsely, based upon the seminal works of Gudmundsson (1994) and Florineth & Schlüchter (2000). Since due its relatively small size no Alpine component is included into the most recent global GIA models as ICE-7G_NA, here we rely upon the high-resolution reconstruction of the Alpine ice sheet during the past glacial cycle proposed by Seguinot *et al.* (2018), which will be referred to as iALP model in the following. This model, based on numerical simulations forced by the GRIP palaeo-temperature records in the alpine region from the Greenland Ice Core Project (Dansgaard *et al.* 1993), provides the ice thickness distribution during the last 120 kyrs BP on a grid with a horizontal spacing of 2 km; a few snapshots of the iALP ice chronology are shown in Fig. 6. In their work, Seguinot *et al.* (2018) also considered other scenarios for the forcing temperature; however, we have verified that adopting these alternative models would not alter the present-day geodetic rates by more than 0.1 mm yr^{-1} across the whole Po Plain. The ice chronology proposed by Seguinot *et al.* (2018), given on a regular cartesian grid, has been converted into disc-shaped axisymmetric elements suitable for use with the TABOO open source post-glacial rebound simulator (Spada *et al.* 2011), by assigning to each disc element an ice height time history obtained as the average over all the grid nodes falling within the disc area. For consistency, the rheological model follows the VM7 viscosity profile by Roy & Peltier (2017), the same adopted to simulate the effects of the far-field ice sheets, described in Section 3.1. The size of the discs is 0.5°, sufficient to capture the main features of model iALP. We have verified that a higher resolution would essentially provide the same results, due to the strong low-pass filter effect that is exerted by the elastic lithosphere and to the fact that possible artifacts due to the discretization of the load would only affect predicted observables at distances from the load comparable to the size of the disc.

We remark that while the effect of global GIA is obtained by means of a gravitationally and topographycally self-consistent solution of the SLE, the regional effects due to the melting of the Würm Alpine ice sheet have been modeled adopting a simplified approach in which the geoid term is neglected and the approximation $\dot{S} \simeq -\dot{U}$ is assumed. As discussed by Spada & Stocchi (2006) and Spada *et al.* (2009) this approximation is valid in the vicinity to the previously glaciated regions and allows a simplified evaluation of sea-level change in response to the melting of small ice sheets.

4 RESULTS

In this section, we discuss the numerical results obtained by means of the GIA models described in Section 3, focusing on the present-day effects on the rates of relative sea-level change ($\dot{S}$), of vertical land motion ($\dot{U}$) and of absolute sea-level change ($\dot{N}$). These fields are sometimes referred to as GIA fingerprints (Plag *et al.* 2001; Spada 2017) and their spatial variability reflects the global effects of deformation, gravitational attraction and rotation within the system composed by the solid Earth, the oceans and the ice sheets (Clark *et al.* 1978; Mitrovica & Milne 2002; Spada & Melini 2019a, b).

4.1 Sea-level change

Fig. 7 shows the present-day rate of sea-level change $\dot{S}$ across the Mediterranean basin according to the ICE-7G_NA (VM7) GIA model. If GIA from the melting of past ice sheets was the unique cause of contemporary sea-level change, those rates would directly manifest as long term sea-level trends at tide gauges. Since GIA evolves on the time scales of millennia, the trends are nearly constant on periods of decades or centuries (e.g. Spada 2017).

The pattern in Fig. 7, whose general features are well known from previous studies of GIA, has been recently reconsidered and discussed by Spada & Melini (2022). The expected maximum rates occur at the center of the sub-basins, with values of $\dot{S}$ up to $\sim$0.3 mm yr^{-1} in the Balearic Sea, up to $\sim$0.2 mm yr^{-1} in the Ionian and in the Levantine Sea and up to $\sim$0.05 mm yr^{-1} in the Black Sea. As pointed out by Spada & Melini (2022), these rates constitute a significant fraction of the trends observed at tide gauges facing these sub-basins. The spatial variability of $\dot{S}$ across the Mediterranean is explained in terms of the ongoing flexure of the lithosphere induced by the melt-water loading, causing a sea-level rise relative to the seafloor. Predicted $\dot{S}$ values decrease and vanish along the southern coasts of the Mediterranean between Algeria, Tunisia, Libya and south Israel. Remarkably, in the Adriatic Sea $\dot{S}$ changes its sign and a sea-level fall ($\dot{S} < 0$) is expected due to GIA, with rates between -0.34 and -0.38 mm yr^{-1} in the Adriatic Sea facing the Venetian

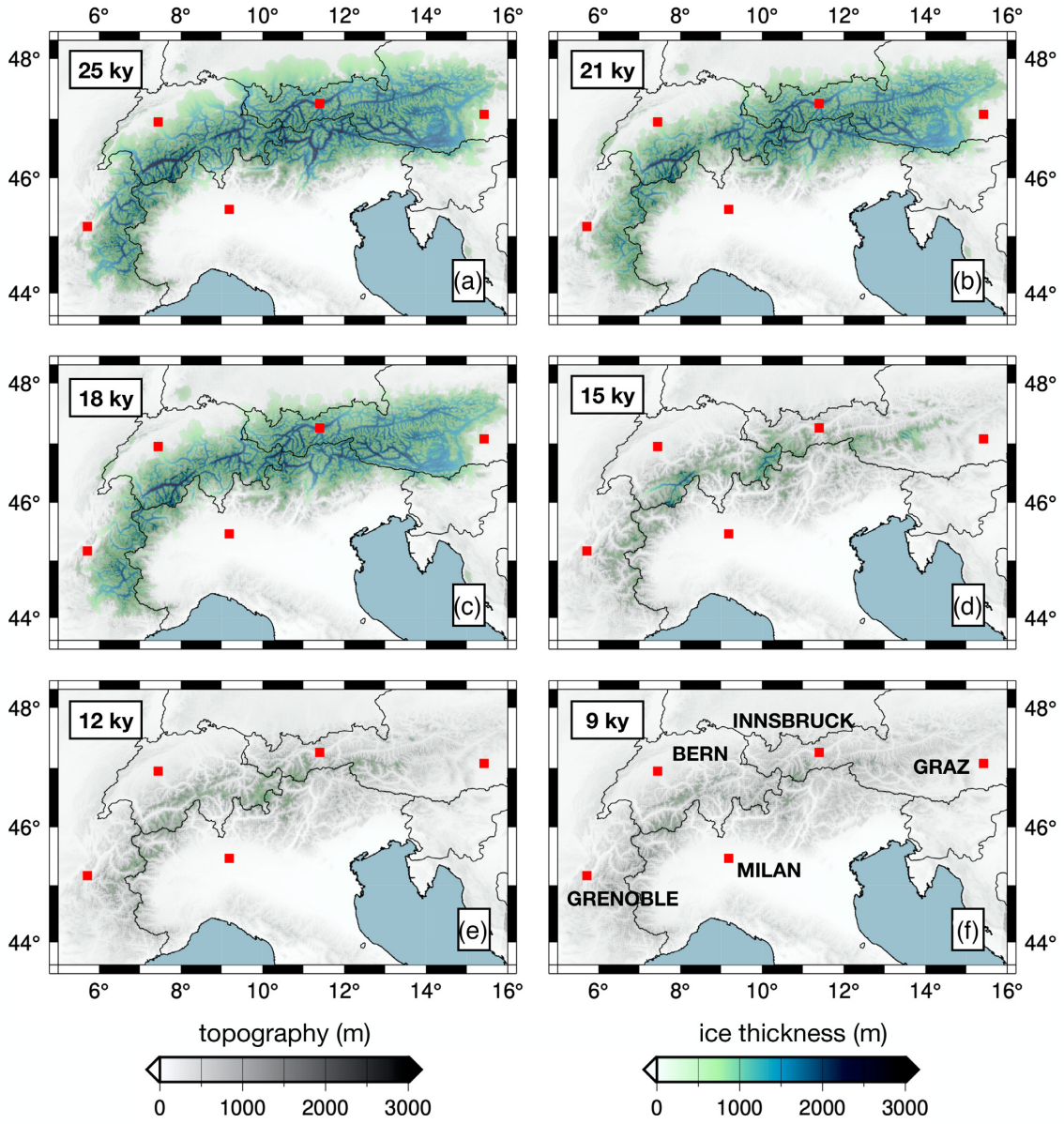

Figure 6. Ice thickness and extents of the Alpine ice sheet according to Seguinot *et al.* (2018), at 26 kyr BP (a), 21 kyr BP (b), 18 kyr BP (c), 15 kyr BP (d), 12 kyr BP (e) and 9 kyr BP (f). Red squares indicate the location of major cities.

Lagoon. A similar pattern is observed in other narrow coastal inlets, as discussed by Spada & Melini (2022). We remark that the rates in Fig. 7 are significantly different from those obtained by Carminati & Di Donato (1999), based upon the ICE-3G(VM1) GIA model by Tushingham & Peltier (1991). This testifies that GIA predictions are not given once for all, but they evolve according to improvements in the knowledge about the chronology of the late-Pleistocene ice sheets and on the mantle viscosity profile and steps forwards in the numerical techniques employed to solve the SLE (see e.g. Spada 2017; Spada & Melini 2022).

Fig. 8 shows the contributions of the ICE-7G_NA (VM7) and iALP models to $\dot{S}$ and $\dot{U}$ GIA fingerprints in the Venice Lagoon, as well as the cumulative effect of the two models. When only the melting of remote ice sheets is considered (Fig. 8a), $\dot{S}$ varies, in the study area, between -0.38 mm yr^{-1} (Venezia and Trieste) and -0.29 mm yr^{-1} (Rimini) and goes further down to -0.22 mm yr^{-1} south of Ancona. These rates are different with respect to previous results by Stocchi & Spada (2009), who obtained positive $\dot{S}$ values across the Mediterranean region. This is to be attributed to the different GIA model assumed by Stocchi & Spada (2009), who employed ICE-5G(VM2) by Peltier (2004) and to the higher spatial resolution of the numerical solution of the SLE adopted in the present study.

The melting of the Alpine glacier (Fig. 8c) is also responsible for a sea-level fall across the northern Adriatic region, albeit of slightly smaller amplitude with respect to that due to global GIA. Modeled rates of sea-level change decrease from north to south, from about -0.30 mm yr^{-1} (Venezia and Trieste) to about -0.12 mm yr^{-1} (Rimini and Pula) and reach zero south of Ancona. Therefore, the melting of the Würm Alpine ice sheet further enhances the sea-level fall associated to continental levering due to the melting of remote ice sheets. Indeed, the cumulated effect of the ICE-7G_NA (VM7) and iALP models, shown in Fig. 8(e), is a general sea-level fall in

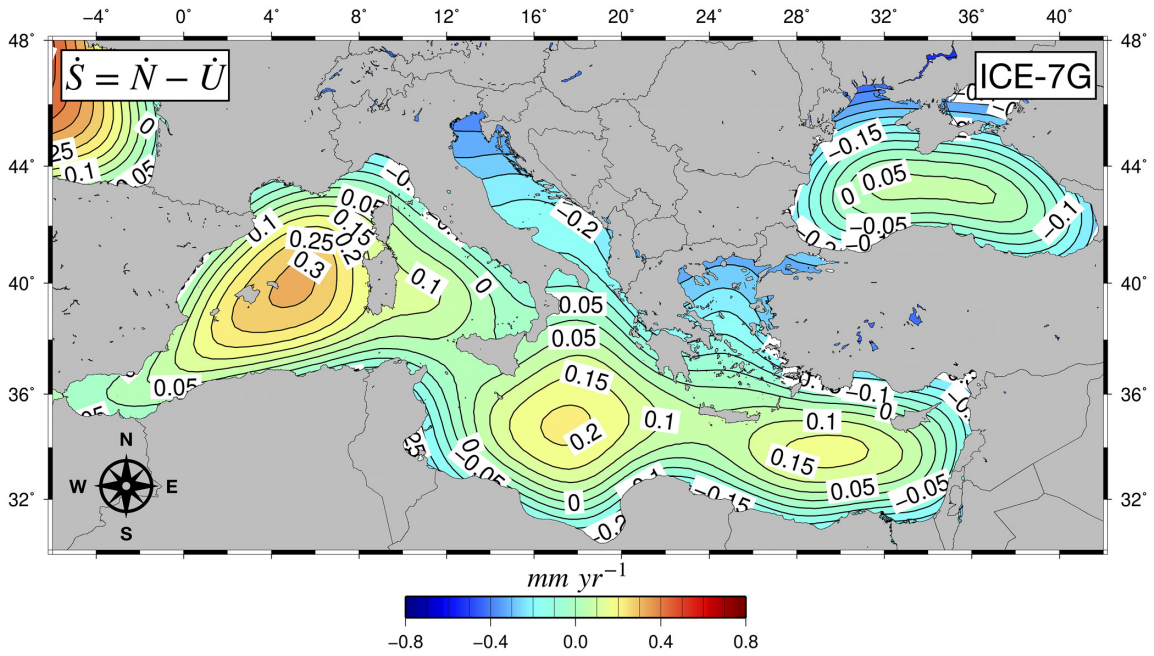

Figure 7. Predicted rate of present-day sea-level change $\dot{S}$ induced by GIA across the Mediterranean region, according to model ICE-7G_NA (VM7). Numerical results have been obtained using the SELEN^4 SLE solver.

the study area, with $\dot{S}$ values ranging from about -0.7 mm yr^{-1} (Venezia and Trieste) to about -0.3 mm yr^{-1} (Rimini) and reaching the -0.2 mm yr^{-1} level south of Ancona, where only the contribution due to global GIA is significant due to the large distance from the Alps. Therefore, it is clear that taking into account the iALP model is essential for a careful reconstruction of the GIA-driven sea-level change in the Venetian Lagoon region.

It is of particular importance here to compare modeled estimates for the GIA contribution to the rate of sea-level change with the observed rates that we discussed in Section 2.1. For Venezia Punta della Salute, the longest-spanning (1909–2000) tide gauge record among those available in the PSMSL database, the observed rate is (2.4 ± 0.2) mm yr^{-1}. Taking into account that the GIA-induced sea-level fall at this site is of about -0.7 mm yr^{-1}, resulting from the combined effect of near-field and remote ice sheets, we would obtain a GIA-corrected rate of sea-level rise of about 3.1 mm yr^{-1}. The contribution of GIA to sea-level change is even more important at Trieste, where a smaller rate of (1.2 ± 0.1) mm yr^{-1} is observed; taking GIA into account, we would obtain a corrected rate of about 1.9 mm yr^{-1}. Modeling the effect of GIA is therefore important for a correct interpretation of the various factors that are contributing to contemporary sea-level change in the Northern Adriatic and in the Venetian Lagoon.

4.2 Vertical land motion

In Fig. 8(b) we show the predicted vertical velocity $\dot{U}$ according to the GIA model ICE-7G_NA (VM7). The GIA fingerprint $\dot{U}$ represents the present-day rate of vertical land motion that would be observed, at a given location, by an earthbound GNSS receiver. In the Venetian Lagoon, predicted uplift rates for ICE-7G_NA (VM7) are in the range between 0.05 and 0.10 mm yr^{-1}, slightly different than those obtained by Carminati & Di Donato (1999) and Stocchi & Spada (2009), based on models ICE-3G (VM1) and ICE-5G (VM2), respectively. Moving southward, vertical velocities predicted by ICE-7G_NA (VM7) decrease and turn into a subsidence with rates of -0.05 mm yr^{-1} between Rimini and Zara and -0.10 mm yr^{-1} south of Ancona. We point out that ICE-7G_NA (VM7) predicts a relative sea-level *fall* (Fig. 8a) even in the subsiding region of the study area (Fig. 8b). This apparent paradox is allowed by the SLE since the relationship $\dot{S} = \dot{N} - \dot{U}$ holds true (see Spada & Melini 2019a) and therefore the conditions $\dot{S} < 0$ and $\dot{U} < 0$ can be simultaneously verified for suitable values of the rate of absolute sea-level change $\dot{N}$.

Fig. 8(d) shows the modeled vertical velocities due to the melting of the Würm Alpine glaciers. Over the northern Adriatic Sea these rates largely exceed those due to global GIA and therefore represent the dominant contribution to GIA-induced vertical land motion in the study area. Indeed, model iALP predicts uplift rates $\dot{U}$ around 0.3 mm yr^{-1} in the Venetian Lagoon and in the range between 0.2 and 0.1 mm yr^{-1} across the most part of the northern Adriatic (Rimini and Pula). The uplift velocities rapidly decay when moving southward, as the distance from the former ice load increases, with rates reaching zero south of Ancona.

The total effect of ICE-7G_NA (VM7) and iALP on the predicted present-day vertical velocity $\dot{U}$ is shown in Fig. 8(f). The rate of vertical land motion varies between 0.4 mm yr^{-1} (Venezia and Trieste) to 0.2 and 0.1 mm yr^{-1} (Rimini and Pula) and reaches zero south of Ancona, turning to a subsidence in the southern part of Adriatic Sea. The pattern of vertical land motion in the study area is largely dominated by the contribution of iALP, confirming the importance of taking into account the melting of the Würm Alpine glaciers to model GIA effects on geodetic observables in the region.

Table 1 lists modeled vertical velocities at the 45 GNSS sites considered in this study due to the combined GIA effect of the ICE-7G_NA (VM7) and iALP models. Rates of vertical land motion due to GIA are generally smaller than the uncertainties associated to the MIDAS estimate of the observed velocity. However, the impact of GIA on observed velocities is generally not negligible; indeed, the average GIA-induced rate of vertical land motion over the 45 considered GNSS sites is $+0.37$ mm yr^{-1}, representing about 28 per cent

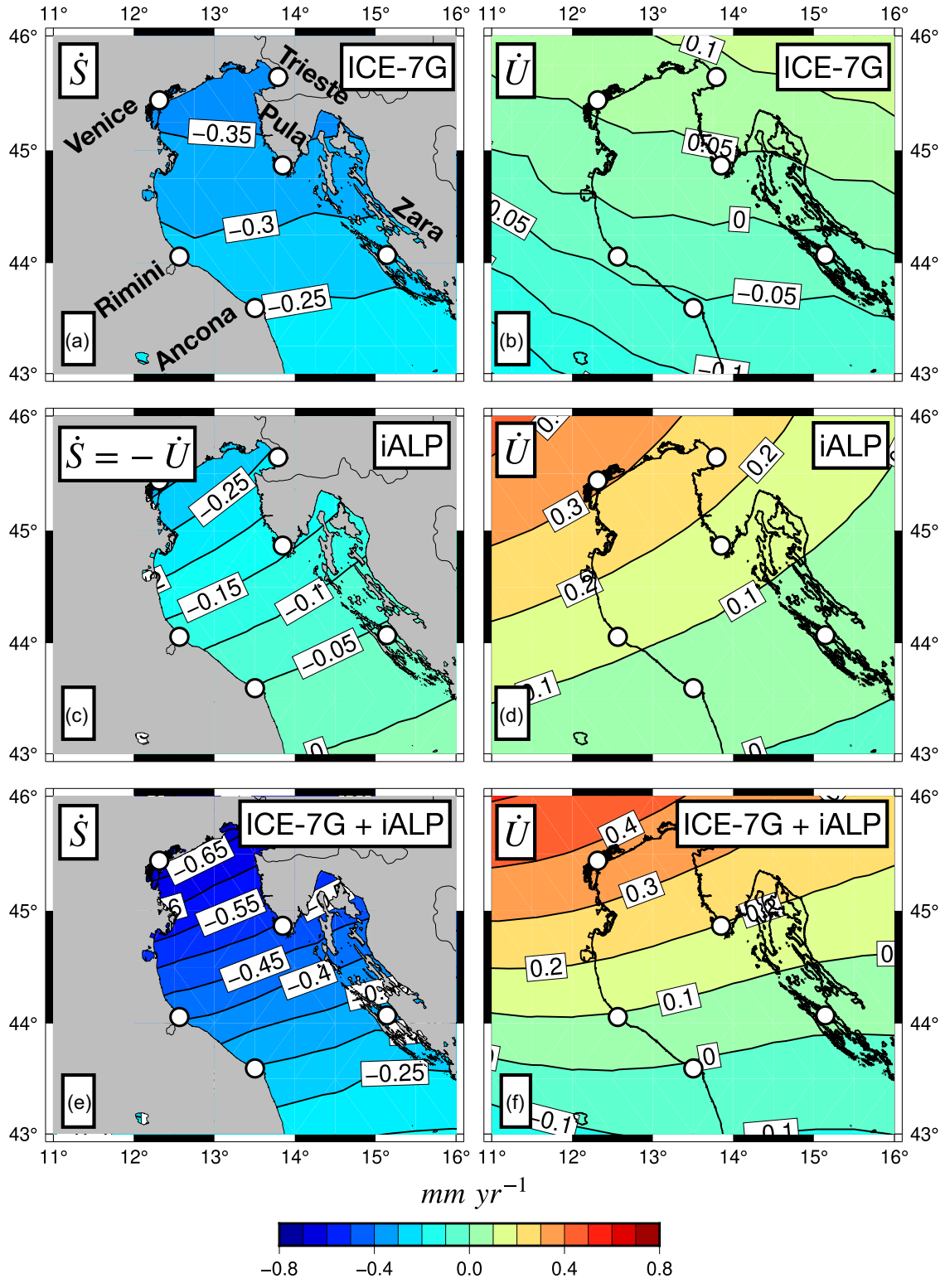

Figure 8. Modeled GIA fingerprints $\dot{S}$ (left frames) and $\dot{U}$ (right) in the Northern Adriatic. Top frames (a–b) show predictions according to the global GIA model ICE-7G_NA (VM7), middle frames (c–d) those obtained with the iALP regional GIA model and bottom frames (e-f) the total effect due to the ICE-7G_NA (VM7) and iALP GIA models. Results shown in frames (a) and (b) have been obtained using the SELEN^4 SLE solver, while those in frames (c) and (d) have been computed with the TABOO code.

of the average vertical velocity (-1.35 mm yr^{-1}) of the GNSS sites listed in Table 1. Only at sites where the largest subsidence rates are recorded (e.g. MST1, TGPO and PTO1), GIA-induced rates represent a second-order contribution to present-day land movements.

4.3 Absolute sea-level

The last GIA fingerprint we consider is $\dot{N}$, the present-day rate of change of the sea surface height (or absolute sea-level). If only GIA was contributing to contemporary sea-level change, $\dot{N}$ would be directly observed by satellite altimetry (Cazenave & Llovel 2010; Bamber & Riva 2010). As we discussed in Section 3.1, the $\dot{N}$ fingerprint is related to $\dot{S}$ and $\dot{U}$ by $\dot{S} = \dot{N} - \dot{U}$. Fig. 9 shows the rate of sea surface height $\dot{N}$ due to global GIA, according to the ICE-7G_NA (VM7) model. The spatial pattern of $\dot{N}$ is characterized by a much smoother variability when compared with $\dot{S}$ and $\dot{U}$ (Stocchi & Spada 2009). Its amplitude is close to -0.3 mm yr^{-1}, the global ocean average of $\dot{N}$ often adopted as a rule of thumb in satellite altimetry (Tamisiea 2011; Spada 2017). We cannot estimate an $\dot{N}$ GIA fingerprint for model iALP since, as discussed in Section 3.2, we are neglecting the geoid term in our approach to regional GIA modeling. In the northern Adriatic and in the Venetian Lagoon, as discussed in Section 2.1, satellite altimetry hints to a sea surface rise between $+4$ and $+6$ mm yr^{-1}, a range that lies above the global mean of $+3$ mm yr^{-1} during the 'altimetry era'. These rates are only marginally affected by GIA, which induces a sea surface fall of about -0.3 mm yr^{-1}, approximately uniform throughout the region.

5 DISCUSSION

Studying sea-level change and vertical land motions in the northern Adriatic Sea, and in particular in the Venetian Lagoon, is of paramount importance in view of the highly vulnerable coastal environments. Accurate modeling of the impact of GIA on these observables is a key factor to allow the identification of the various geophysical contributions which are driving the measured rates.

In Section 4, we have shown that the pattern of present-day GIA-induced rates of sea-level change in the Mediterranean is characterized by positive values in the bulk of the basin, with peak values of $\dot{S}$ of about 0.3 mm yr^{-1}, due to the sea floor subsidence associated to the melt-water load (Mitrovica & Milne 2002; Stocchi & Spada 2007). On the contrary, in the northern Adriatic Sea, our global GIA model predicts a sea-level fall with rates between -0.38 mm yr^{-1} (Venice and Trieste) and -0.26 mm yr^{-1} (Ancona). As discussed in detail by Spada & Melini (2022), negative values of $\dot{S}$ are common in narrow sub-basins, where the coastal profiles are characterized by a short radius of curvature and can be explained in terms of continental levering (see e.g. Mitrovica & Milne 2002). The vertical velocity field induced by the ongoing effects of global GIA is characterized by a tilting pattern, with the northern coast of the Adriatic (between Venezia and Trieste) uplifting at rates between 0.05 and 0.10 mm yr^{-1}, while the southern part of the study area (south of Ancona) is subsiding at a rate of about -0.1 mm yr^{-1}. If we take into account the contributions from both global and regional GIA, our model predicts a widespread sea-level fall in the northern Adriatic, with rates decreasing southward from -0.7 mm yr^{-1} between Venezia and Trieste to -0.2 mm yr^{-1} south of Ancona and an uplift field with vertical velocities of about 0.4 mm yr^{-1} on the northern margin of the basin, which decrease southward reaching the zero level at Ancona.

Sea-level rise and vertical land motion in the northern Adriatic is the result of a wide range of geophysical, geological and anthropogenic effects. As we have shown, modeling GIA effects in the region is of key importance to correctly identify the drivers of observed sea-level rise and to interpret measured velocities at GNSS stations. For an accurate GIA modeling, the isostatic response to the melting of the Alpine Würm ice sheet needs to be taken into account. Of course, GIA models are not given once and for all and further elements need to be included in the future. For instance, due to lateral variations in the rheological properties of the Earth, GIA is a fully 3-D global problem; this is especially true in regions like the Mediterranean basin, characterized by structural heterogeneities due to its complex geodynamical setting (Sternai *et al.* 2019). Furthermore, as pointed out in the seminal work by Piromallo & Morelli (1997), the Alps structure at depth shows significant differences between the western and eastern sections of the arc, possibly reflecting a difference in past subduction of the Tethyan lithosphere and subsequent continental collision. In this respect, a fully 3-D regional GIA model may possibly explain, at least in part, the horizontal gradients in vertical geodetic velocities and sea-level rates in the Northern Adriatic. However, the computational complexity of a 3-D numerical approach to the GIA problem is such that only few attempts to 3-D GIA models have been discussed in literature (see e.g. Li *et al.* 2020). Moreover, uncertainties on the details of the ice load evolution also affect GIA predictions (Melini & Spada 2019). In this respect, uplift estimates from GIA models in the Alpine region in the presence of lateral rheological variations are still a matter of discussion.

6 CONCLUSIONS

In this work, we have obtained an up-to-date, high-resolution estimate of sea-level change and vertical deformation at the Mediterranean scale, based upon the ICE-7G_NA (VM7) GIA model of Roy & Peltier (2018) and a reconstruction of the time evolution of the Alpine ice sheet during the last glacial phase obtained by Seguinot *et al.* (2018). To estimate present-day geodetic fingerprints, we combined an high resolution, global solution of the SLE describing the topographically and gravitationally self-consistent response to the melting of late-Pleistocene ice complexes with an approximated approach suitable for modeling the regional-scale effects associated with the Alpine ice sheet. Indeed, due to its proximity to the Alpine arc, the northern Adriatic region is expected to be significantly affected by near-field isostatic effects associated with the melting of the Alpine Würm ice sheet. Our results show that regional GIA in response to the melting of near-field ice sheets further enhances the sea-level fall associated with global GIA and represents the dominant GIA contribution to vertical land motion in the northern Adriatic with uplift rates up to 0.3 mm yr^{-1} on the coast between Venezia and Trieste.

By comparing vertical velocities provided by our GIA model with observed rates at GNSS sites, we find that GIA effects are a marginal contribution to geodetic velocity only at sites where the largest subsidence is recorded. Conversely, at the majority of GNSS sites, GIA may represent a significant contribution to observed rates and shall be taken into account for a correct interpretation of the velocity field. Similarly, GIA-driven sea-level change represents a fraction of the observed rates of sea-level ranging from 30 per cent in the Venetian Lagoon to over 50 per cent at Trieste and it significantly mitigates sea-level rise due to present-day climate change, to the

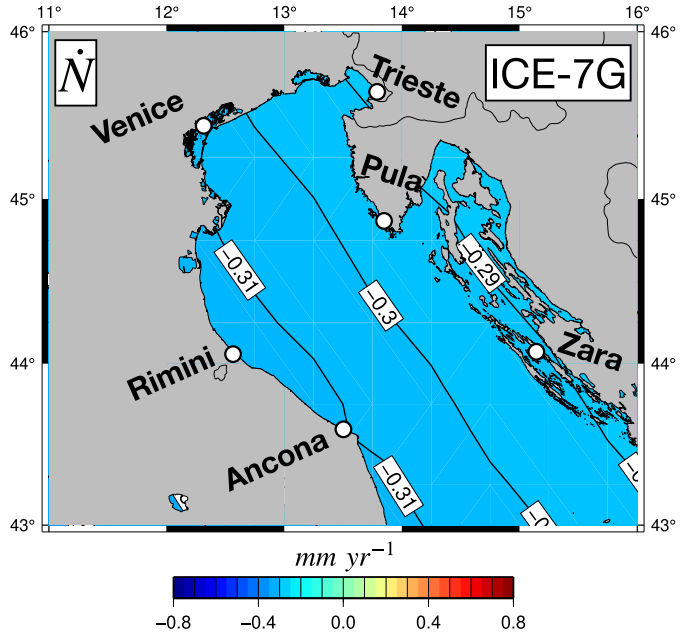

Figure 9. Predicted present-day rate of change of the sea surface height $\dot{N}$ in the north Adriatic sea, according to model ICE-7G_NA (VM7). The computation have been performed using program SELEN[4].

natural compaction of recent fine-grained alluvial deposits and to anthropic activities like the extraction of underground fluids.

GIA models are constantly evolving as knowledge about the spatio-temporal evolution of late-Pleistocene ice sheets and on the mantle viscosity improves and as new numerical techniques are developed. The Mediterranean region is characterized by a complex geodynamical setting and structural heterogeneities beneath the Alpine arc are well known from tomographic evidences. A next generation of GIA models, based on a fully 3-D numerical approach to the GIA problem, will allow a more accurate modeling of GIA fingerprints in the Northern Adriatic.

ACKNOWLEDGMENTS

We thank two anonymous Reviewers and the Editor for their insightful and constructive comments that considerably helped improving the original manuscript. All figures have been drawn using the Generic Mapping Tools (GMT) of Wessel and Smith (1998). We acknowledge PSMSL for making available the tide gauge data from http://www.psmsl.org. The Nevada Geodetic Laboratory is acknowledged for making available the GPS data from the web page http://geodesy.unr.edu/index.php. We acknowledge Prof WR Peltier for making available data about the spatio-temporal evolution of ice sheets according to model ICE-7G_NA on the web page https://www.atmosp.physics.utoronto.ca/~peltier/data.php. We thank Open Physics Hub (OPH) of DIFA (Dipartimento di Fisica e Astronomia 'Augusto Righi') of the Alma Mater Studiorum Università di Bologna for providing support with the Data Analysis cluster 'BladeRunner' hosted in the Tier-1 server room of the INFN-CNAF. This work is partly supported by the INGV project Pianeta Dinamico 2021-22 Tema 4 KINDLE (grant no. CUP D53J19000170001), funded by the Italian Ministry of University and Research 'Fondo finalizzato al rilancio degli investimenti delle amministrazioni centrali dello Stato e allo sviluppo del Paese, legge 145/2018'.

DATA AVAILABILITY

Program SELEN[4] (SELEN version 4.0) is available from the Computational Infrastructure for Geodynamics (CIG) at https://github.com/geodynamics/selen. The Post Glacial Rebound Solver TABOO can be downloaded from https://github.com/danielemelini/TABOO. The MIDAS algorithm code is available from the Nevada Geodetic Laboratory (NGL) at the link http://geodesy.unr.edu/MIDAS_release/?C=M;O=A. Numerical data underlying all figures shown in this work are available upon request to the corresponding author.

REFERENCES

Amante, C. & Eakins, B.W., 2009. ETOPO1 1 arc-minute global relief model: procedures, data sources and analysis. NOAA technical memorandum NESDIS NGDC-24, *National Geophysical Data Center, NOAA,* **10**(2009), 1–19.

Bamber, J. & Riva, R., 2010. The sea level fingerprint of recent ice mass fluxes, *The Cryosphere,* **4**(4), 621–627.

Blewitt, G. & Lavallée, D., 2002. Effect of annual signals on geodetic velocity, *J. Geophys. Res.: Solid Earth,* **107**(B7), ETG–9. doi:10.1029/2001JB000570.

Blewitt, G., Kreemer, C., Hammond, W.C. & Gazeaux, J., 2016. MIDAS robust trend estimator for accurate GPS station velocities without step detection, *J. Geophys. Res.: Solid Earth,* **121**(3), 2054–2068.

Brambati, A., Carbognin, L., Quaia, T., Teatini, P. & Tosi, L., 2003. The Lagoon of Venice: geological setting, evolution and land subsidence, *Episodes,* **26**(3), 264–268.

Buble, G., Bennett, R. & Hreinsdóttir, S., 2010. Tide gauge and GPS measurements of crustal motion and sea level rise along the eastern margin of Adria, *J. Geophys. Res.: Solid Earth,* **115**(B2). doi:10.1029/2008JB006155.

Camuffo, D. & Sturaro, G., 2003. Sixty-cm submersion of Venice discovered thanks to Canaletto's paintings, *Climatic Change,* **58**(3), 333–343.

Carbognin, L., Teatini, P. & Tosi, L., 2009. The impact of relative sea level rise on the Northern Adriatic Sea coast, Italy, *WIT Trans. Ecology Environment,* **127,** 137–148.

Carbognin, L., Teatini, P., Tomasin, A. & Tosi, L., 2010. Global change and relative sea level rise at Venice: what impact in term of flooding, *Climate Dynamics,* **35**(6), 1039–1047.

Carminati, E. & Di Donato, G., 1999. Separating natural and anthropogenic vertical movements in fast subsiding areas: the Po plain (N. Italy) case, *Geophys. Res. Lett.,* **26**(15), 2291–2294.

Caron, L., Ivins, E., Larour, E., Adhikari, S., Nilsson, J. & Blewitt, G., 2018. GIA model statistics for GRACE hydrology, cryosphere and ocean science, *Geophys. Res. Lett.,* **45**(5), 2203–2212.

Cazenave, A. & Llovel, W., 2010. Contemporary sea level rise, *Annu. Rev. Mar. Sci.,* **2,** 145–173.

Cazenave, A., Palanisamy, H. & Ablain, M., 2018. Contemporary sea level changes from satellite altimetry: What have we learned? What are the new challenges?, *Adv. Space Res.,* **62**(7), 1639–1653.

Clark, J.A. & Lingle, C.S., 1979. Predicted relative sea-level changes (18,000 years BP to present) caused by late-glacial retreat of the Antarctic ice sheet, *Quat. Res.,* **11**(3), 279–298.

Clark, J.A., Farrell, W.E. & Peltier, W.R., 1978. Global changes in postglacial sea level: A numerical calculation1, *Quat. Res.,* **9**(3), 265–287.

Dansgaard, W. *et al.*, 1993. Evidence for general instability of past climate from a 250-kyr ice-core record, *Nature,* **364**(6434), 218–220.

Davis, J., Bennett, R. & Wernicke, B., 2003. Assessment of GPS velocity accuracy for the Basin and Range Geodetic Network (BARGEN), *Geophys. Res. Lett.,* **30**(7). doi:10.1029/2003GL016961.

Douglas, B.C., 1991. Global sea level rise, *J. Geophys. Res.: Oceans,* **96**(C4), 6981–6992.

Douglas, B.C., 1997. Global sea rise: a redetermination, *Surv. Geophys.,* **18**(2), 279–292.

Emery, K., Aubrey, D. & Goldsmith, V., 1988. Coastal neo-tectonics of the Mediterranean from tide-gauge records, *Mar. Geol.,* **81**(1–4), 41–52.

Farrell, W. & Clark, J.A., 1976. On postglacial sea level, *J. geophys. Int.,* **46**(3), 647–667.

Florineth, D. & Schlüchter, C., 2000. Alpine evidence for atmospheric circulation patterns in Europe during the Last Glacial Maximum, *Quat. Res.,* **54**(3), 295–308.

Fouache, E., Faivre, S., Dufaure, J.-J., Kovacic, V. & Tassaux, F., 2000. New observations on the evolution of the Croatian shoreline between Poreç and Zadar over the past 2000 years, *Z. Geomorphologie. Supplementband,* **122,** 33–46.

Galassi, G. & Spada, G., 2014. Linear and non-linear sea-level variations in the Adriatic Sea from tide gauge records (1872–2012), *Ann. Geophys.,* **57**(6). doi:10.4401/ag-6536.

Gatto, P. & Carbognin, L., 1981. The Lagoon of Venice: natural environmental trend and man-induced modification/La Lagune de Venise: l'évolution naturelle et les modifications humaines, *Hydrol. Sci. J.,* **26**(4), 379–391.

Gudmundsson, G.H., 1994. An order-of-magnitude estimate of the current uplift-rates in Switzerland caused by the Würm Alpine deglaciation, *Eclogae Geologicae Helvetiae,* **87**(2), 545–557. https://doi.org/10.5169/seals-167470

Hammond, W.C., Blewitt, G. & Kreemer, C., 2016. GPS imaging of vertical land motion in California and Nevada: Implications for Sierra Nevada uplift, *J. Geophys. Res.: Solid Earth,* **121**(10), 7681–7703.

Kreemer, C. & Blewitt, G., 2021. Robust estimation of spatially varying common-mode components in GPS time-series, *J. Geod.,* **95**(1), 1–19.

Kreemer, C. & Zaliapin, I., 2018. Spatiotemporal correlation between seasonal variations in seismicity and horizontal dilatational strain in California, *Geophys. Res. Lett.,* **45**(18), 9559–9568.

Kreemer, C., Hammond, W.C. & Blewitt, G., 2018. A robust estimation of the 3-D intraplate deformation of the North American plate from GPS, *J. Geophys. Res.: Solid Earth,* **123**(5), 4388–4412.

Lambeck, K., Antonioli, F., Anzidei, M., Ferranti, L., Leoni, G., Scicchitano, G. & Silenzi, S., 2011. Sea level change along the Italian coast during the Holocene and projections for the future, *Quat. Int.,* **232**(1–2), 250–257.

Legeais, J.-F. *et al.*, 2018. An improved and homogeneous altimeter sea level record from the ESA Climate Change Initiative, *Earth System Sci. Data,* **10**(1), 281–301.

Li, T. *et al.*, 2020. Uncertainties of glacial isostatic adjustment model predictions in North America associated with 3D structure, *Geophys. Res. Lett.,* **47,** e2020GL087944. doi:10.1029/2020GL087944.

Lionello, P., Nicholls, R.J., Umgiesser, G. & Zanchettin, D., 2021. Venice flooding and sea level: past evolution, present issues and future projections (introduction to the special issue), *Natural Hazards Earth System Sci.,* **21**(8), 2633–2641.

Marcos, M. & Tsimplis, M., 2007. Variations of the seasonal sea level cycle in southern Europe, *J. Geophys. Res.: Oceans,* **112**(C12). doi:10.1029/2006JC004049.

Marcos, M. & Tsimplis, M.N., 2008. Coastal sea level trends in Southern Europe, *J. geophys. Int.,* **175**(1), 70–82.

Melini, D. & Spada, G., 2019. Some remarks on glacial isostatic adjustment modelling uncertainties, *J. geophys. Int.,* **218**(1), 401–413.

Michel, A., Santamaría-Gómez, A., Boy, J.-P., Perosanz, F. & Loyer, S., 2021. Analysis of GNSS displacements in Europe and their comparison with hydrological loading models, *Remote Sensing,* **13**(22), 4523. doi:10.3390/rs13224523.

Mitrovica, J. & Milne, G., 2002. On the origin of late Holocene sea-level highstands within equatorial ocean basins, *Quat. Sci. Rev.,* **21**(20–22), 2179–2190.

Mitrovica, J.X. & Wahr, J., 2011. Ice age earth rotation, *Annu. Rev. Earth Planet. Sci.,* **39,** 577–616.

Mitrovica, J.X., Wahr, J., Matsuyama, I. & Paulson, A., 2005. The rotational stability of an ice-age earth, *J. geophys. Int.,* **161**(2), 491–506.

Murray, K., Murray, M. & Sheehan, A., 2019. Active deformation near the Rio Grande Rift and Colorado Plateau as inferred from continuous Global Positioning System measurements, *J. Geophys. Res.: Solid Earth,* **124**(2), 2166–2183.

Ojo, A.O., Kao, H., Jiang, Y., Craymer, M. & Henton, J., 2021. Strain accumulation and release rate in Canada: implications for long-term crustal deformation and earthquake hazards, *J. Geophys. Res.: Solid Earth,* **126**(4), e2020JB020529. doi:10.1029/2020JB020529.

Peltier, W., 2004. Global glacial isostasy and the surface of the ice-age Earth: The ICE-5G (VM2) Model and GRACE, *Annu. Rev. Earth Planet. Sci.,* **32**(1), 111–149.

Piromallo, C. & Morelli, A., 1997. Imaging the mediterranean upper mantle by p-wave travel time tomography, *Ann. Geophys.,* **40**(4). 963–979.

Plag, H.P., Juettner, H.U., *et al.*, 2001. Inversion of global tide gauge data for present-day ice load changes, Proceedings of the Second International Symposium on Environmental Research in the Arctic and Fifth Ny-Ålesund Scientific Seminar: Memoirs of the National Institute of Polar Research, Special Issue 54, pp. 301–317.

Rocco, F.V., 2015. Sea level trends in the Mediterranean from tide gauges and satellite altimetry, Ph.D. thesis, Alma Mater Studiorum, University of Bologna, Italy. http://amslaurea.unibo.it/10172/.

Roy, K. & Peltier, W., 2015. Glacial isostatic adjustment, relative sea level history and mantle viscosity: reconciling relative sea level model predictions for the US East coast with geological constraints, *J. geophys. Int.,* **201**(2), 1156–1181.

Roy, K. & Peltier, W., 2017. Space-geodetic and water level gauge constraints on continental uplift and tilting over North America: regional convergence of the ICE-6G_C (VM5a/VM6) models, *J. geophys. Int.,* **210**(2), 1115–1142.

Roy, K. & Peltier, W., 2018. Relative sea level in the Western Mediterranean basin: A regional test of the ICE-7G_NA (VM7) model and a constraint on late Holocene Antarctic deglaciation, *Quat. Sci. Rev.,* **183,** 76–87.

Seguinot, J., Ivy-Ochs, S., Jouvet, G., Huss, M., Funk, M. & Preusser, F., 2018. Modelling last glacial cycle ice dynamics in the Alps, *The Cryosphere,* **12**(10), 3265–3285.

Sen, P.K., 1968. Estimates of the regression coefficient based on Kendall's tau, *J. Am. Stat. Assoc.,* **63**(324), 1379–1389.

Spada, G., 2017. Glacial isostatic adjustment and contemporary sea level rise: An overview, *Surv. Geophys.,* **38**(1), 153–185.

Spada, G. & Melini, D., 2019a. On some properties of the glacial isostatic adjustment fingerprints, *Water,* **11**(9), 1844. doi:10.3390/w11091844.

Spada, G. & Melini, D., 2019b. SELEN 4 (SELEN version 4.0): a Fortran program for solving the gravitationally and topographically self-consistent sea-level equation in glacial isostatic adjustment modeling, *Geoscientific Model Dev.,* **12**(12), 5055–5075.

Spada, G. & Melini, D., 2022. New estimates of ongoing sea level change and land movements caused by glacial isostatic adjustment in the mediterranean region, *J. geophys. Int.,* **229**(2), 984–998.

Spada, G. & Stocchi, P., 2006. *The Sea Level Equation, Theory and Numerical Examples,* Aracne Editrice, Roma.

Spada, G. & Stocchi, P., 2007. SELEN: A Fortran 90 program for solving the "sea-level equation", *Comput. Geosci.,* **33**(4), 538–562.

Spada, G., Stocchi, P. & Colleoni, F., 2009. Glacio–isostatic adjustment in the Po plain and in the northern adriatic region, *Pure Appl. Geophys.,* **166**(8), 1303–1318.

Spada, G. *et al.*, 2011. A benchmark study for glacial isostatic adjustment codes, *J. geophys. Int.,* **185**(1), 106–132.

Sternai, P. *et al.*, 2019. Present-day uplift of the european alps: Evaluating mechanisms and models of their relative contributions, *Earth Sci. Rev.,* **190,** 589–604.

Stocchi, P. & Spada, G., 2007. Post-glacial sea-level in the Mediterranean Sea: Clark's zones and role of remote ice sheets, *Ann. Geophys,* **50**(6), 741–761. https://doi.org/10.4401/ag-3054

Stocchi, P. & Spada, G., 2009. Influence of glacial isostatic adjustment upon current sea level variations in the Mediterranean, *Tectonophysics,* **474**(1–2), 56–68.

Stocchi, P., Spada, G. & Cianetti, S., 2005. Isostatic rebound following the Alpine deglaciation: impact on the sea level variations and vertical movements in the Mediterranean region, *J. geophys. Int.,* **162**(1), 137–147.

Tamisiea, M.E., 2011. Ongoing glacial isostatic contributions to observations of sea level change, *J. geophys. Int.,* **186**(3), 1036–1044.

Tegmark, M., 1996. An icosahedron-based method for pixelizing the celestial sphere, *Astrophys. J.,* **470**(2), L81.

Theil, H., 1950. A rank-invariant method of linear and polynomial regression analysis, *Indagationes mathematicae,* **12**(85), 173.

Tsimplis, M. & Spencer, N., 1997. Collection and analysis of monthly mean sea level data in the Mediterranean and the Black Sea, *J. Coast. Res.,* **13,** 534–544.

Tsimplis, M.N., Raicich, F., Fenoglio-Marc, L., Shaw, A.G., Marcos, M., Somot, S. & Bergamasco, A., 2012. Recent developments in understanding sea level rise at the adriatic coasts, *Physics and Chemistry of the Earth, Parts A/B/C,* **40,** 59–71.

Tushingham, A. & Peltier, W., 1991. ICE-3G: A new global model of late Pleistocene deglaciation based upon geophysical predictions of post-glacial relative sea level change, *J. Geophys. Res.: Solid Earth,* **96**(B3), 4497–4523.

Vignudelli, S., Birol, F., Benveniste, J., Fu, L.-L., Picot, N., Raynal, M. & Roinard, H., 2019. Satellite altimetry measurements of sea level in the coastal zone, *Surveys in Geophysics,* **40**(6), 1319–1349.

Wessel, P. & Smith, W.H., 1998. New, improved version of Generic Mapping Tools released, *EOS Trans. Am. Geophys. Union,* **79**(47), 579–579.

Whitehouse, P.L., 2018. Glacial isostatic adjustment modelling: historical perspectives, recent advances and future directions, *Earth Surface Dynamics,* **6**(2), 401–429.

Yu, C., Li, Z., Penna, N.T. & Crippa, P., 2018. Generic atmospheric correction model for interferometric synthetic aperture radar observations, *J. Geophys. Res.: Solid Earth,* **123**(10), 9202–9222.

Zanchettin, D. *et al.*, 2021. Sea-level rise in Venice: historic and future trends, *Natural Hazards Earth Syst. Sci.,* **21**(8), 2643–2678.